Correlated x-ray and electron beam steering by pulse-front tilt in laser wakefield acceleration

Erik Löfquist, Cornelia Gustafsson, Andrea Angella, Anders Persson, and Olle Lundh*

Division of Atomic Physics, Department of Physics, Lund University, Lund, Sweden

(Received 27 June 2025; accepted 10 October 2025; published 30 October 2025)

Laser wakefield accelerators produce ultrashort, highly relativistic electron and x-ray pulses in plasma over millimeter distances. Crucial for investigations and applications of these pulses is a reproducible and controlled output beam pointing. Even with a perfectly stable laser, pulse-front tilt in the driving laser pulse has been shown to cause both the laser pulse and the electron beam to deviate differently from the optical axis after the plasma. We show that this steering also extends to the generated x-rays, but in such a way that they perfectly follow the electron beam. The electron beam or x-ray beam pointing can thus be noninvasively inferred from the other, even when pulse-front-tilt steering is present. This enables active stabilization of either beam, without significant impact on key beam parameters such as energy, charge, and divergence.

DOI: 10.1103/cq83-8kfb

I. INTRODUCTION

Laser wakefield acceleration (LWFA) [1,2] attracts significant interest as a compact method for generating femtosecond [3] multi-GeV [4–7] electron bunches. These bunches have both direct applications in radiotherapy [8,9] and can be used to produce secondary radiation with plasma lenses [10], as well as conventional accelerator insertion devices, with proof-of-principle experiments even demonstrating free electron lasing [11–13]. At the same time, the betatron x-ray pulses emitted during LWFA itself are also of interest [14] and has been used in pump-probe studies of warm dense matter [15,16], phase contrast imaging [17–21], and absorption imaging [22,23]. Many properties of the electron beam can be inferred from the x-ray beam and vice versa [24–29].

Beneficial for any application is a well-defined and tunable output beam pointing. To first approximation, the output electron and x-ray pulses propagate collinearly with the driving laser pulse along the optical axis, which in this paper refers to the propagation axis of the laser beam in the absence of a plasma. However, in the presence of a transverse electron density gradient or when the laser pulse exhibits a pulse-front tilt (PFT), the laser pulse and the electron beam can deviate from the optical axis by up to several tens of milliradians [30–34].

Pulse-front tilt is a first order spatiotemporal coupling, i.e., the pulse intensity cannot be described as the product of spatial and temporal envelopes [35]. With PFT, the intensity is tilted in space with respect to the propagation axis. PFT can arise from angular chirp or from a combination of spatial chirp and group delay dispersion (GDD) [36]. When focused, the PFT rotates in the plane of the tilt, and the peak intensity is reduced compared to that of a beam without PFT, as the angular chirp becomes a spatial chirp in the focus [37]. For LWFA, the ponderomotive force from a laser pulse exhibiting PFT excites an asymmetric plasma wave. As the PFT rotates around the focus, the plasma wave and any trapped electrons follow transversely, leading to a deflection from the optical axis [31].

PFT steering of the electron beam was first demonstrated in the nonlinear LWFA regime, explained by the transverse plasma electron density formed by the tilted laser pulse [30]. Simulations also showed that the laser beam deflects, along with the entire accelerating structure, and that the PFT leads to off-axis injection and collective betatron oscillations. This was experimentally corroborated by measurements proving that the polarization state of the x-rays can be controlled by the orientation of the PFT [38], as well as by measurements showing that the laser deflection deviates from the electron deflection [32]. PFT steering of the laser and electron beams has also been shown in simulation for the linear regime of LWFA, where analytical models for predicting the deflection exist [31,32].

In this article, we complement previous studies by experimentally examining the pointing of the x-ray beam and its correlation to the PFT-steered electron beam pointing. Parallels to related physics observed when steering in transverse plasma gradients are also discussed [39,40].

*Contact author: olle.lundh@fysik.lu.se.

Published by the American Physical Society under the terms of the Creative Commons Attribution 4.0 International license. Further distribution of this work must maintain attribution to the author(s) and the published article's title, journal citation, and DOI.

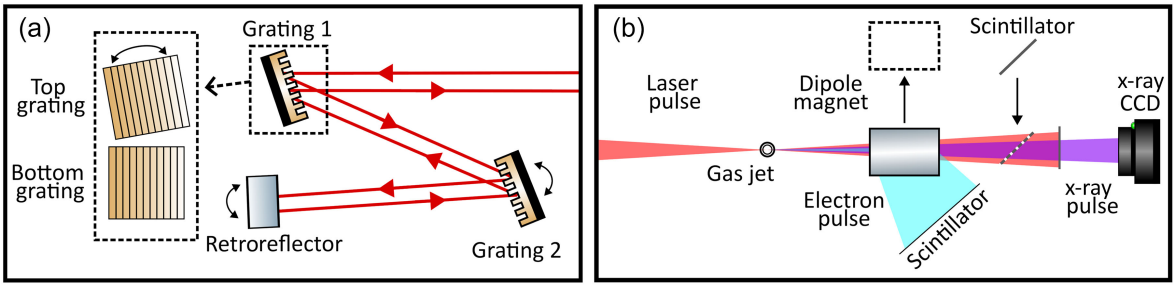


FIG. 1. (a) Compressor geometry and beam path viewed from above. The returning beam from the retroreflector propagates at a lower height and has been displaced horizontally in the figure for clarity. The first grating pair is shown to the left, viewed head on. Solid black arrows indicate introduced rotations. All misalignments are greatly exaggerated. (b) Top view of the LWFA setup. The focused laser pulse generates electrons and x-rays in the gas jet. In one diagnostic configuration, the electrons are dispersed by the dipole magnet onto a scintillator, measuring the energy spectrum and pointing vertically, while the x-ray profile is simultaneously recorded in the forward direction. Alternatively, to image the electron beam profile in both transverse directions, the magnet is removed and another scintillator inserted directly into the beam path, as indicated by vertical arrows and dashed lines.

II. METHOD

The multiterawatt Ti:Sapphire laser at Lund Laser Centre delivers 1 J compressed laser pulses on target, horizontally polarized, with a duration of 40 fs and a center wavelength of 800 nm. The laser pulse propagates in vacuum and is focused by an f/13 off-axis parabolic mirror at the entrance to a 1.5 mm supersonic gas jet. The focal spot size of an attenuated beam is measured to have a 12 μm full width at half maximum. The maximum normalized laser vector potential is estimated to be 2.3 in vacuum, with no self-focusing. Electrons are continuously injected throughout acceleration by ionization injection [41,42], as opposed to the self-injection used in previous studies of PFT in LWFA [30,32,38]. The gas mixture is composed of 99% helium and 1% nitrogen, leading to a peak electron number density on axis of 6.2×10^{18} cm^{-3}, assuming fully ionized helium and 5 times ionized nitrogen.

All relative PFT changes are introduced in the Treacy double-pass grating compressor [43] of the chirped pulse amplification system, whose geometry is shown in Fig. 1(a). A difference from the standard configuration is that grating 1, corresponding to the first and final reflections, is composed of two separate gratings. PFT in the horizontal dispersion plane is introduced, akin to Popp *et al.* [30], by changing the angle of incidence on grating 2 in the dispersion plane and compensating the pointing offset with the retroreflector. PFT vertically, out of the dispersion plane, is introduced by slightly rotating the top section of grating 1, in the plane of the grating itself, similarly to the work by Mittelberger *et al.* [32]. Beam pointing in this case is corrected using a motorized mirror after the compressor. When turning any grating, the position of the attenuated focal spot is monitored on a camera. This is used to realign the laser to the same optical axis, with an accuracy limited by laser pointing fluctuations of 5 μrad. This procedure mitigates motor hysteresis effects, ensuring a well-defined grating rotation between each setting. In the presence of an angular chirp, GDD also affects the PFT [36]. The GDD is tuned by varying the distance between the grating pair.

The electron spectrum was measured as indicated in Fig. 1(b), by dispersing the electrons horizontally (in the dispersion plane of the compressor and parallel to the laser polarization) with a 0.8 T permanent dipole magnet onto a scintillating screen. This enables energy-dependent pointing measurements out of the dispersion plane. At the same time, the x-ray beam profile and pointing was measured in the forward direction by a back-illuminated deep depletion x-ray camera. A second diagnostic configuration, in which the dipole magnet and x-ray CCD are removed and a scintillating screen is inserted into the beam path, was used to measure the electron beam pointing and profile in both transverse directions. All pointings were determined with 2D Gaussian fits to the beam profiles.

Nominal electron beams were fully polychromatic up to a maximum energy of 200 MeV, estimated as the point where the spectrum drops below 0.1 pC/MeV. Above 20 MeV, the mean energy was 90 MeV and the total charge was 150 pC.

III. RESULTS

Sample electron beam profiles are shown in Fig. 2 for five different vertical angular chirps separated by 0.2 μrad/nm. The vertical deflection, in the plane of the PFT, is clearly evident, with a total steering up to 50 mrad demonstrated here. The energy resolved vertical pointing is illustrated in Fig. 3 together with the corresponding generated x-ray profiles. Electrons across the entire polychromatic spectrum is deflected with similar output pointing, and the steering also extends to the x-ray beam.

The averaged vertical pointing is shown in Fig. 4 for the x-ray beam in red crosses and the electrons in blue circles as a function of relative angular chirp and grating in-plane rotation, with ten shots at each setting. The electron beam

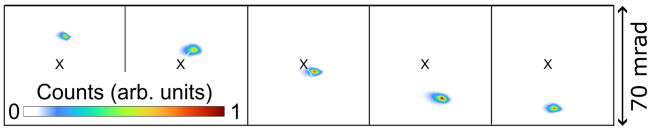


FIG. 2. Electron beam profiles for vertical angular chirp, varied in steps of 0.2 μrad/nm from left to route. Black crosses mark the optical axis, and the angular scale (shown to the right) is identical in both dimensions. A clear steering of up to 50 mrad is observed in the plane of the pulse-front tilt.

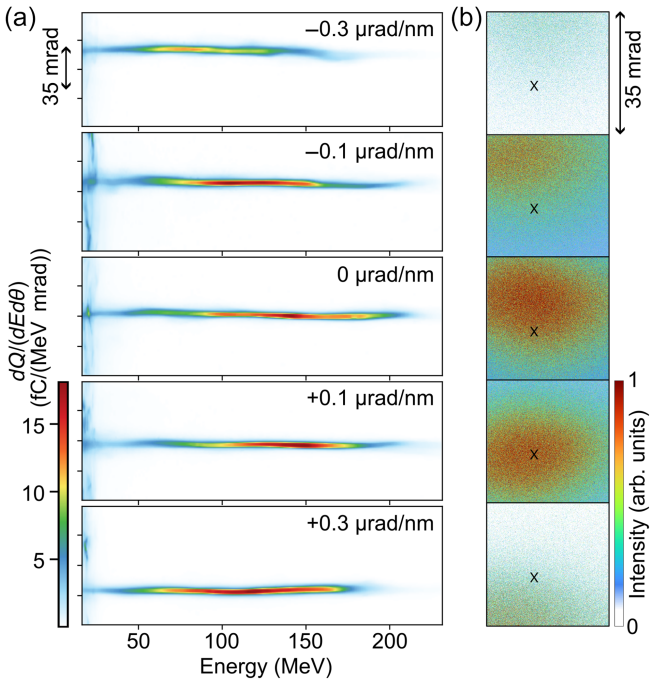


FIG. 3. (a) Example electron spectra for five different incident vertical angular chirps, given in the top right. Electrons reach a maximum energy of 200 MeV. The angular scale illustrates deflection in the plane of the pulse-front tilt, which does not significantly depend on the electron energy. (b) The corresponding x-ray profiles generated by the electron beams in (a). Black crosses mark the optical axis, and the field of view is smaller than in the electron spectra, indicated by the angular scale in the top right. The signal in the two outermost x-ray images (where the centroid misses the camera) has been multiplied by 4 to aid visibility. The x-ray beam pointing follows the same trend as that of the electron beams.

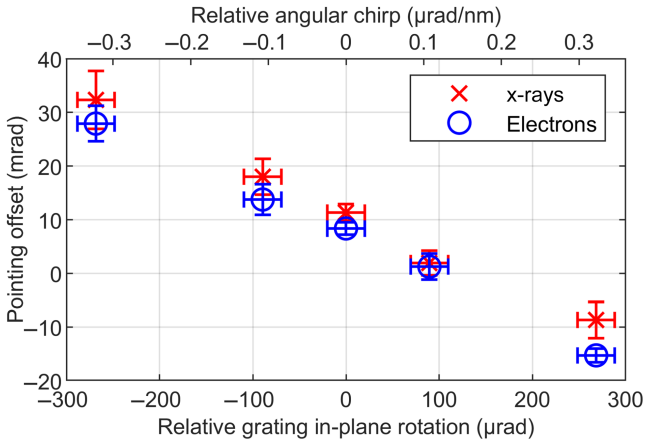


FIG. 4. Vertical pointing offset from the optical axis for the x-ray beam in red crosses, and the electron beam in blue circles, shown as a function of relative angular chirp and grating in-plane rotation angle. Vertical error bars correspond to the standard deviation from the mean for the ten shots at each position. The two curves are roughly linear and follow each other closely.

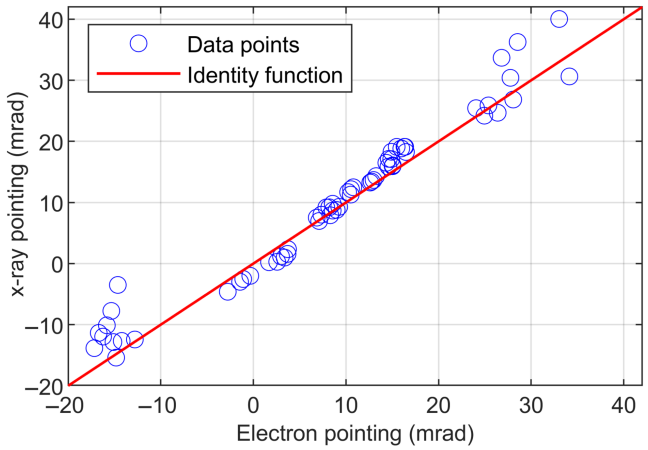


FIG. 5. Scatterplot of the x-ray pointing as a function of the electron beam pointing, for the data in Fig. 4. Each blue circle corresponds to a single shot, while the red line is the identity function, drawn as a guide to the eye. Near perfect correlation is clearly seen not only in the mean pointing, but also on a shot-to-shot basis.

was optimized for maximum energy around the center of the scan. Since no absolute measurement of the angular chirp was taken, the pointing offset from the optical axis at the center of the scan could indicate a compressor misalignment at the starting conditions, or that the laser pulse had acquired a small amount of angular chirp already before entering the compressor. No significant difference is seen between the pointing of the x-rays and the electrons, both displaying a linear trend in the studied regime. The magnitude of the slope is 65 mrad/(μrad/nm), which for this particular compressor gives a slope of 80 μrad/μrad with respect to the relative grating in-plane rotation. Very slight compressor misalignments can thus give large deflections from the optical axis. The 50 mrad deflection is 2 orders of magnitude larger than the electron pointing jitter of 0.6 mrad, which is in turn 2 orders of magnitude larger than the 5 μrad pointing jitter of the laser.

Since the vertical deflections of the electron and x-ray beam are recorded simultaneously, the shot-by-shot correlation between the two beam directions can be examined. This is shown in Fig. 5, with the x-ray pointing plotted as a function of the electron pointing, shot-by-shot, in blue circles. The identity line, shown by the red line as a guide to

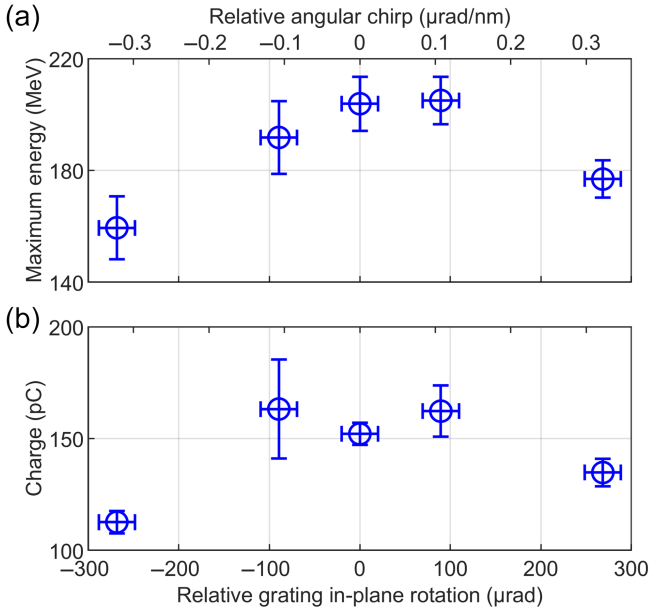


FIG. 6. Maximum electron beam energy in (a), and total charge in (b), plotted as a function of relative angular chirp and corresponding grating in-plane rotation. For the three central points, no trends larger than the shot-to-shot fluctuations are seen. Each data point consist of ten shots.

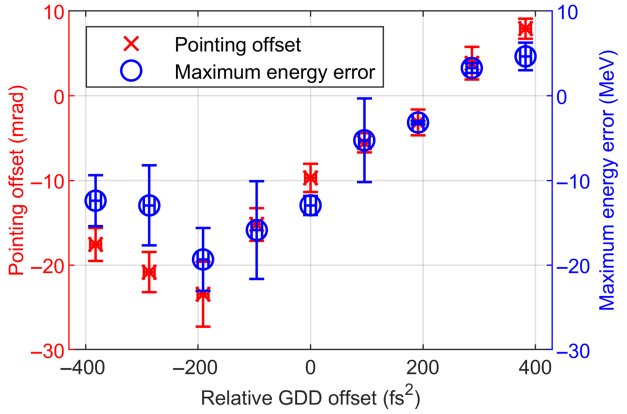


FIG. 7. Horizontal pointing offset in red crosses, shown as a function of a relative GDD shift. Taking the measured pointing offset into account when analyzing the energy spectrometer data, leads to an offset in maximum energy compared to the case where the electrons had been assumed to be on the optical axis. This error is shown in blue circles and corresponds up to 10% of the final energy of 200 MeV. Each data point consists of six shots.

the eye, closely matches the data, which has a Pearson coefficient of 0.978. The larger uncertainty at the two extreme ends, is due to the pointing deviations being so large that the centroid of the x-ray beam misses the camera, leading to a more uncertain fit [this corresponds to the two edge cases in Fig. 3(b)]. Excluding these points, the Pearson coefficient improves to 0.994.

No significant energy-dependent pointing variation is observed, despite the continuous ionization injection mechanism. The final electron pointing is thus not directly coupled to the electron beam pointing at the point of injection. This is consistent with the interpretation that the entire accelerating structure deflect along with the laser beam in the plasma. Figure 6 shows two electron beam characteristics—maximum energy in (a), and charge in (b), as functions of the relative angular chirp (top) and corresponding grating in-plane rotation (bottom). Apart from the two outermost sampled angular chirps, these electron beam characteristics do not change significantly compared to the shot-to-shot fluctuations. This demonstrates the possibility for active pointing stabilization of the electron and x-ray beams within ±10 mrad, as first proposed by Popp *et al.* [30], even without compensating for the GDD offset that an introduced angular chirp would give at the target [36]. The latter is unsurprising, as the introduced GDD offset is small, less than -1 fs^2, for the angular chirps in this study and the 20 m propagation distance between the compressor and the LWFA target.

As an example application relevant to LWFA studies, we illustrate how knowing the electron beam pointing is useful for correctly interpreting electron beam spectra. Electrons can be deliberately steered in the horizontal dispersion plane of the dipole magnet, by introducing a horizontal PFT to the laser pulse. Figure 7 shows in red crosses the measured pointing offsets as a function of a relative GDD offset, a typical parameter scan that is regularly performed when optimizing LWFA electron beams. Since the deflection is in the dispersion plane, taking the pointing into account when calculating the electron trajectories through the magnet results in an offset in energy compared to the assumption that the electrons enter the magnet along the optical axis. This error is shown for the maximum energy in blue circles, differing by up to 20 MeV, corresponding to around 10% of the maximum energy. While the magnitude of the offset differs for different spectrometers, the example shows that even for our relatively compact spectrometer, where the target, magnet, and scintillating screen are centimeters apart, the effect can be substantial. By inferring the electron beam pointing from the x-ray pointing, this error can be corrected for on a single-shot basis, without the need for a dual-screen electron spectrometer setup [44].

IV. DISCUSSION

Although the observation that electron and x-ray beams are collinear even in the presence of a PFT may seem intuitive at first, we emphasize that this is not always the case. As x-rays are continuously emitted by the electrons during acceleration, and thus during their deflection, one should expect an elongated x-ray beam being emitted in the plane of deflection with different critical energy at different angles, as demonstrated for the case of a transverse plasma gradient (no initial PFT) [39,40]. This would give a collective x-ray pointing closer to the optical axis

than the electron beam. The reason this elongation of the x-ray profile does not significantly affect the output pointing of the x-ray beam is likely because the high-energy electrons dominate the x-ray emission [14]. For continuously accelerated electrons, as in our experiment, the x-ray beam will predominantly be generated at the end of the plasma and thus share the same pointing as the output electron beam. However, if the electrons reach the decelerating phase of the wakefield, known as dephasing, the peak x-ray flux will be emitted at this point instead of at the end of the plasma. If the electrons continue to be steered after dephasing, one could observe a large offset between the pointing of the electron beam and x-ray beam for PFT steering, in analogy to the transverse plasma gradient experiments [39,40].

Lower energy x-rays are partially suppressed in the detection by the filters in the beam path to the camera (3 μm aluminum foil blocking the laser, 50 μm Kapton sealing the vacuum chamber, and 250 μm beryllium in front of the camera chip). This can be used advantageously if one desires to use the x-ray beam to infer the pointing of the electron beam, even in cases where the x-ray profile's elongation is significant. By adjusting the thickness of a thin metal foil in the beam path, it is possible to absorb most of the low-energy photons while maintaining a strong signal at the higher energies, where the correlation is one-to-one between the two beams. This enables live, noninvasive, automated control of the electron (or x-ray) beam pointing, which will have applications, for example, in staging LWFA experiments.

V. CONCLUSION

Electron beam steering in LWFA by tens of milliradians using pulse-front tilt is demonstrated. Despite continuous electron injection, the pointing is insensitive to the electron energy, corroborating that steering arises as the electron beam deflects along with the entire plasma wave transversely. A one-to-one correlation between the LWFA electron and hard betatron x-ray beam pointing is shown to extend to the case of pulse-front tilt steering. This enables noninvasive active stabilization of either beam within several milliradians, without significant impact on key beam parameters.

ACKNOWLEDGMENTS

The authors gratefully acknowledge insightful discussions with Claes-Göran Wahlström on the physics and presentation of the manuscript. This work was supported by funding from the Swedish Research Council (VR 2019-04784, 2024-05698), and the Knut and Alice Wallenberg Foundation (KAW 2019.0318, 2020.0111).

DATA AVAILABILITY

The data that support the findings of this article are not publicly available upon publication because it is not technically feasible and/or the cost of preparing, depositing, and hosting the data would be prohibitive within the terms of this research project. The data are available from the authors upon reasonable request.

[1] T. Tajima and J. M. Dawson, Laser electron accelerator, Phys. Rev. Lett. **43**, 267 (1979).

[2] E. Esarey, C. B. Schroeder, and W. P. Leemans, Physics of laser-driven plasma-based electron accelerators, Rev. Mod. Phys. **81**, 1229 (2009).

[3] O. Lundh, J. Lim, C. Rechatin, L. Ammoura, A. Ben-Ismaïl, X. Davoine, G. Gallot, J. P. Goddet, E. Lefebvre, V. Malka, and J. Faure, Few femtosecond, few kiloampere electron bunch produced by a laser-plasma accelerator, Nat. Phys. **7**, 219 (2011).

[4] A. J. Gonsalves *et al.*, Petawatt laser guiding and electron beam acceleration to 8 GeV in a laser-heated capillary discharge waveguide, Phys. Rev. Lett. **122**, 084801 (2019).

[5] B. Miao, J. E. Shrock, L. Feder, R. C. Hollinger, J. Morrison, R. Nedbailo, A. Picksley, H. Song, S. Wang, J. J. Rocca, and H. M. Milchberg, Multi-GeV electron bunches from an all-optical laser wakefield accelerator, Phys. Rev. X **12**, 031038 (2022).

[6] C. Aniculaesei *et al.*, The acceleration of a high-charge electron bunch to 10 GeV in a 10-cm nanoparticle-assisted wakefield accelerator, Matter Radiat. Extremes **9**, 014001 (2024).

[7] A. Picksley, J. Stackhouse, C. Benedetti, K. Nakamura, H. E. Tsai, R. Li, B. Miao, J. E. Shrock, E. Rockafellow, H. M. Milchberg, C. B. Schroeder, J. Van Tilborg, E. Esarey, C. G. Geddes, and A. J. Gonsalves, Matched guiding and controlled injection in dark-current-free, 10-GeV-class, channel-guided laser-plasma accelerators, Phys. Rev. Lett. **133**, 255001 (2024).

[8] K. Svendsen, D. Guénot, J. B. Svensson, K. Petersson, A. Persson, and O. Lundh, A focused very high energy electron beam for fractionated stereotactic radiotherapy, Sci. Rep. **11**, 5844 (2021).

[9] Z. Guo, S. Liu, B. Zhou, J. Liu, H. Wang, Y. Pi, X. Wang, Y. Mo, B. Guo, J. Hua, Y. Wan, and W. Lu, Preclinical tumor control with a laser-accelerated high-energy electron radiotherapy prototype, Nat. Commun. **16**, 2025 (1895).

[10] J. Björklund Svensson, D. Guénot, J. Ferri, H. Ekerfelt, I. Gallardo González, A. Persson, K. Svendsen, L. Veisz, and O. Lundh, Low-divergence femtosecond x-ray pulses from a passive plasma lens, Nat. Phys. **17**, 639 (2021).

[11] W. Wang, K. Feng, L. Ke, C. Yu, Y. Xu, R. Qi, Y. Chen, Z. Qin, Z. Zhang, M. Fang, J. Liu, K. Jiang, H. Wang, C. Wang, X. Yang, F. Wu, Y. Leng, J. Liu, R. Li, and Z. Xu, Free-electron lasing at 27 nanometres based on a laser wakefield accelerator, Nature (London) **595**, 516 (2021).

[12] M. Labat *et al.*, Seeded free-electron laser driven by a compact laser plasma accelerator, Nat. Photonics **17**, 150 (2023).

[13] S. K. Barber *et al.*, Greater than 1000-fold gain in a free-electron laser driven by a laser-plasma accelerator with high reliability, Phys. Rev. Lett. **135**, 055001 (2025).

[14] S. Corde, K. Ta Phuoc, G. Lambert, R. Fitour, V. Malka, A. Rousse, A. Beck, and E. Lefebvre, Femtosecond x-rays

from laser-plasma accelerators, Rev. Mod. Phys. **85**, 1 (2013).

[15] M. Z. Mo, Z. Chen, S. Fourmaux, A. Saraf, S. Kerr, K. Otani, R. Masoud, J.-C. Kieffer, Y. Tsui, A. Ng, and R. Fedosejevs, Measurements of ionization states in warm dense aluminum with betatron radiation, Phys. Rev. E **95**, 053208 (2017).

[16] B. Mahieu, N. Jourdain, K. Ta Phuoc, F. Dorchies, J.-P. Goddet, A. Lifschitz, P. Renaudin, and L. Lecherbourg, Probing warm dense matter using femtosecond x-ray absorption spectroscopy with a laser-produced betatron source, Nat. Commun. **9**, 3276 (2018).

[17] S. Fourmaux, S. Corde, K. T. Phuoc, P. Lassonde, G. Lebrun, S. Payeur, F. Martin, S. Sebban, V. Malka, A. Rousse, and J. C. Kieffer, Single shot phase contrast imaging using laser-produced betatron x-ray beams, Opt. Lett. **36**, 2426 (2011).

[18] S. Kneip, C. McGuffey, F. Dollar, M. S. Bloom, V. Chvykov, G. Kalintchenko, K. Krushelnick, A. Maksimchuk, S. P. Mangles, T. Matsuoka, Z. Najmudin, C. A. Palmer, J. Schreiber, W. Schumaker, A. G. Thomas, and V. Yanovsky, X-ray phase contrast imaging of biological specimens with femtosecond pulses of betatron radiation from a compact laser plasma wakefield accelerator, Appl. Phys. Lett. **99**, 093701 (2011).

[19] Z. Najmudin, S. Kneip, M. S. Bloom, S. P. Mangles, O. Chekhlov, A. E. Dangor, A. Dopp, K. Ertel, S. J. Hawkes, J. Holloway, C. J. Hooker, J. Jiang, N. C. Lopes, H. Nakamura, P. A. Norreys, P. P. Rajeev, C. Russo, M. J. Streeter, D. R. Symes, and M. Wing, Compact laser accelerators for x-ray phase-contrast imaging, Phil. Trans. R. Soc. A **372**, 20130032 (2014).

[20] J. Wenz, S. Schleede, K. Khrennikov, M. Bech, P. Thibault, M. Heigoldt, F. Pfeiffer, and S. Karsch, Quantitative x-ray phase-contrast microtomography from a compact laser-driven betatron source, Nat. Commun. **6**, 7568 (2015).

[21] K. Svendsen, I. G. González, M. Hansson, J. B. Svensson, H. Ekerfelt, A. Persson, and O. Lundh, Optimization of soft x-ray phase-contrast tomography using a laser wakefield accelerator, Opt. Express **26**, 33930 (2018).

[22] D. Guénot, K. Svendsen, J. Björklund Svensson, H. Ekerfelt, A. Persson, O. Lundh, and E. Berrocal, Simultaneous laser-driven x-ray and two-photon fluorescence imaging of atomizing sprays, Optica **7**, 131 (2020).

[23] D. Guénot, K. Svendsen, B. Lehnert, H. Ulrich, A. Persson, A. Permogorov, L. Zigan, M. Wensing, O. Lundh, and E. Berrocal, Distribution of liquid mass in transient sprays measured using laser-plasma-driven x-ray tomography, Phys. Rev. Appl. **17**, 064056 (2022).

[24] G. R. Plateau, C. G. Geddes, D. B. Thorn, M. Chen, C. Benedetti, E. Esarey, A. J. Gonsalves, N. H. Matlis, K. Nakamura, C. B. Schroeder, S. Shiraishi, T. Sokollik, J. Van Tilborg, C. Toth, S. Trotsenko, T. S. Kim, M. Battaglia, T. Stöhlker, and W. P. Leemans, Low-emittance electron bunches from a laser-plasma accelerator measured using single-shot x-ray spectroscopy, Phys. Rev. Lett. **109**, 064802 (2012).

[25] M. Schnell, A. Sävert, B. Landgraf, M. Reuter, M. Nicolai, O. Jäckel, C. Peth, T. Thiele, O. Jansen, A. Pukhov, O. Willi, M. C. Kaluza, and C. Spielmann, Deducing the electron-beam diameter in a laser-plasma accelerator using x-ray betatron radiation, Phys. Rev. Lett. **108**, 075001 (2012).

[26] S. Kneip, C. McGuffey, J. L. Martins, M. S. Bloom, V. Chvykov, F. Dollar, R. Fonseca, S. Jolly, G. Kalintchenko, K. Krushelnick, A. Maksimchuk, S. P. Mangles, Z. Najmudin, C. A. Palmer, K. T. Phuoc, W. Schumaker, L. O. Silva, J. Vieira, V. Yanovsky, and A. G. Thomas, Characterization of transverse beam emittance of electrons from a laser-plasma wakefield accelerator in the bubble regime using betatron x-ray radiation, Phys. Rev. ST Accel. Beams **15**, 021302 (2012).

[27] C. Thaury, E. Guillaume, S. Corde, R. Lehe, M. Le Bouteiller, K. Ta Phuoc, X. Davoine, J. M. Rax, A. Rousse, and V. Malka, Angular-momentum evolution in laser-plasma accelerators, Phys. Rev. Lett. **111**, 135002 (2013).

[28] A. Curcio, M. Anania, F. Bisesto, E. Chiadroni, A. Cianchi, M. Ferrario, F. Filippi, D. Giulietti, A. Marocchino, M. Petrarca, V. Shpakov, and A. Zigler, Trace-space reconstruction of low-emittance electron beams through betatron radiation in laser-plasma accelerators, Phys. Rev. Accel. Beams **20**, 012801 (2017).

[29] A. Curcio, M. Anania, F. Bisesto, E. Chiadroni, A. Cianchi, M. Ferrario, F. Filippi, D. Giulietti, A. Marocchino, F. Mira, M. Petrarca, V. Shpakov, and A. Zigler, Single-shot non-intercepting profile monitor of plasma-accelerated electron beams with nanometric resolution, Appl. Phys. Lett. **111**, 133105 (2017).

[30] A. Popp, J. Vieira, J. Osterhoff, Z. Major, R. Hörlein, M. Fuchs, R. Weingartner, T. P. Rowlands-Rees, M. Marti, R. A. Fonseca, S. F. Martins, L. O. Silva, S. M. Hooker, F. Krausz, F. Grüner, and S. Karsch, All-optical steering of laser-wakefield-accelerated electron beams, Phys. Rev. Lett. **105**, 215001 (2010).

[31] M. Thévenet, D. E. Mittelberger, K. Nakamura, R. Lehe, C. B. Schroeder, J.-L. Vay, E. Esarey, and W. P. Leemans, Pulse front tilt steering in laser plasma accelerators, Phys. Rev. Accel. Beams **22**, 071301 (2019).

[32] D. E. Mittelberger, M. Thévenet, K. Nakamura, A. J. Gonsalves, C. Benedetti, J. Daniels, S. Steinke, R. Lehe, J. L. Vay, C. B. Schroeder, E. Esarey, and W. P. Leemans, Laser and electron deflection from transverse asymmetries in laser-plasma accelerators, Phys. Rev. E **100**, 063208 (2019).

[33] S. Mishra, B. S. Rao, A. Moorti, and J. A. Chakera, Enhanced betatron x-ray emission in a laser wakefield accelerator and wiggler due to collective oscillations of electrons, Phys. Rev. Accel. Beams **25**, 090703 (2022).

[34] S. Mishra, B. S. Rao, A. Moorti, and J. A. Chakera, High brightness betatron x-ray source driven by chirped laser pulses, Phys. Plasmas **31**, 103105 (2024).

[35] S. W. Jolly, O. Gobert, and F. Quéré, Spatio-temporal characterization of ultrashort laser beams: A tutorial, J. Opt. **22**, 103501 (2020).

[36] S. Akturk, X. Gu, E. Zeek, and R. Trebino, Pulse-front tilt caused by spatial and temporal chirp, Opt. Express **12**, 4399(2004).

[37] G. Pretzler, A. Kasper, and K. J. Witte, Angular chirp and tilted light pulses in CPA lasers, Appl. Phys. B **70**, 1 (2000).

[38] M. Schnell, A. Sävert, I. Uschmann, M. Reuter, M. Nicolai, T. Kämpfer, B. Landgraf, O. Jäckel, O. Jansen, A. Pukhov, M. C. Kaluza, and C. Spielmann, Optical control of hard x-ray polarization by electron injection in a laser wakefield accelerator, Nat. Commun. **4**, 2421 (2013).

[39] Y. Ma, D. Seipt, S. J. Dann, M. J. Streeter, C. A. Palmer, L. Willingale, and A. G. Thomas, Angular streaking of betatron x-rays in a transverse density gradient laser-wakefield accelerator, Phys. Plasmas **25**, 113105 (2018).

[40] Y. Ma, J. A. Cardarelli, P. T. Campbell, S. Fourmaux, R. Fitzgarrald, M. D. Balcazar, A. F. Antoine, N. F. Beier, Q. Qian, A. E. Hussein, B. Kettle, S. R. Klein, K. Krushelnick, Y. F. Li, S. P. Mangles, G. Sarri, D. Seipt, V. Senthilkumaran, M. J. Streeter, L. Willingale, and A. G. Thomas, Single-shot diagnosis of electron energy evolution via streaked betatron x-rays in a curved laser wakefield accelerator, Phys. Rev. Lett. **132**, 225001 (2024).

[41] A. Pak, K. A. Marsh, S. F. Martins, W. Lu, W. B. Mori, and C. Joshi, Injection and trapping of tunnel-ionized electrons into laser-produced wakes, Phys. Rev. Lett. **104**, 025003 (2010).

[42] C. McGuffey, A. G. Thomas, W. Schumaker, T. Matsuoka, V. Chvykov, F. J. Dollar, G. Kalintchenko, V. Yanovsky, A. Maksimchuk, K. Krushelnick, V. Y. Bychenkov, I. V. Glazyrin, and A. V. Karpeev, Ionization induced trapping in a laser wakefield accelerator, Phys. Rev. Lett. **104**, 025004 (2010).

[43] E. Treacy, Optical pulse compression with diffraction gratings, IEEE J. Quantum Electron. **5**, 454 (1969).

[44] I. Blumenfeld, C. E. Clayton, F.-J. Decker, M. J. Hogan, C. Huang, R. Ischebeck, R. Iverson, C. Joshi, T. Katsouleas, N. Kirby, W. Lu, K. A. Marsh, W. B. Mori, P. Muggli, E. Oz, R. H. Siemann, D. Walz, and M. Zhou, Energy doubling of 42 GeV electrons in a metre-scale plasma wakefield accelerator, Nature (London) **445**, 741 (2007).